JOURNAL OF COMPUTATIONAL PHYSICS 103, 286–299 (1992)

A Cell-Centered Lagrangian-Mesh Diffusion Differencing Scheme

J. E. MOREL, J. E. DENDY, JR., MICHAEL L. HALL, AND STEPHEN W. WHITE

University of California, Los Alamos National Laboratory, Los Alamos, New Mexico 87545

Received November 1, 1990; revised November 27, 1991

A new cell-centered diffusion differencing scheme for the quadrilateral meshes associated with Lagrangian hydrodynamics codes is described. Computational comparisons of this scheme and existing schemes are given. It is shown that the new scheme is much more accurate than existing schemes when the mesh is significantly skewed. The new scheme is also more costly because there are special cell-edge unknowns in addition to the standard cell-center unknowns, and the associated diffusion matrix is asymmetric. The disadvantages of an asymmetric diffusion matrix are mitigated by a multigrid solution technique that is quite effective. © 1992 Academic Press, Inc.

1. INTRODUCTION

There are several different schemes for solving the diffusion equation on the quadrilateral meshes associated with Lagrangian hydrodynamics codes. For instance, Kershaw [1] and Pert [2] have respectively developed cell-centered variational and finite-difference methods based upon a smooth mapping between the logical mesh coordinates and the spatial coordinates. Unfortunately, the meshes that appear in hydrodynamics calculations are rarely smooth. Thus these schemes can give poor results for such calculations. Finite element methods do not require a smooth mapping between the logical and spatial coordinates, but the unknowns must be placed at cell corners rather than cell centers, and this can cause considerable difficulty in coupling such schemes with standard Lagrangian hydrodynamic codes [3].

We have developed a cell-centered diffusion differencing scheme that is fully compatible with standard Lagrangian hydrodynamics codes and has many desirable properties. Specifically:

1. The scheme is equivalent to the standard five-point cell-centered scheme on an orthogonal mesh.
2. Local energy conservation is maintained over each Lagrangian cell.
3. Material discontinuities are rigorously treated.
4. The method preserves the homogeneous linear solutions $a+bx+cy$ and $a+br+cz$ in $x-y$ and $r-z$ geometries, respectively.
5. The numerical solution converges to the exact solution in the limit as the mesh is refined, regardless of the smoothness of the mesh.
6. The method gives second-order accuracy.

To our knowledge, no other scheme has previously been proposed with all of these properties. However, the scheme also has two disadvantages:

1. There are cell-edge unknowns in addition to the cell-center unknowns.
2. The diffusion matrix is asymmetric.

Even though there are cell-edge unknowns, we refer to our scheme as cell-centered because the time-derivative and absorption terms are "lumped" with respect to the cell-center unknowns. That is to say, that only the cell-center unknowns appear in these terms. Thus initial conditions for the edge unknowns are not required. This property is necessary to maintain strict compatibility with standard Lagrangian hydrodynamics codes. The asymmetry of the diffusion matrix is potentially a serious drawback of our method. Many modern schemes for solving the diffusion equation can fail if the diffusion matrix is not symmetric and positive-definite. However, we have developed a multigrid method for solving our scheme that is quite effective. Thus the most significant disadvantage of an asymmetric diffusion matrix is avoided. A disadvantage of the asymmetry that cannot be avoided results from the need for pivoting in the Gaussian elimination process. This increases the work associated with the multigrid relaxation process and inhibits vectorization. One must be concerned about temporal instability with an asymmetric diffusion matrix, but extensive computational testing indicates that such instabilities are not a problem with our method. Our diffusion matrix can become ill-conditioned if the mesh is sufficiently distorted, but we have a simple modification of the scheme that maintains good conditioning in this situation without a serious loss of accuracy. We stress that this modification

0021-9991/92 $5.00
Copyright © 1992 by Academic Press, Inc.
All rights of reproduction in any form reserved.

need only be applied in cases of extreme cell distortion, and the effects of this modification tend to be quite localized.

The primary purpose of this paper is threefold: to derive our scheme, to present a multigrid method for solving our equations, and to give computational results for certain standard problems which demonstrate the accuracy and robustness of our scheme relative to existing cell-centered schemes.

The remainder of this paper is organized as follows. In Section 2 we derive our basic differencing scheme. In Section 3 we discuss the effect of cell distortions on this basic scheme and describe a modification of the scheme that allows us to deal with extremely distorted cells. In Section 4 we discuss both a simple line-relaxation technique that can be used to solve our equations efficiently when small time steps are being taken and a multigrid method that can be used to solve our equations efficiently under all conditions. Computational results are given in Section 5, followed by conclusions in Section 6.

2. DERIVATION OF THE BASIC DIFFERENCING SCHEME

In this section our basic diffusion differencing scheme is derived. We begin with the equations that we wish to solve,

$$\frac{1}{v}\frac{\partial \phi}{\partial t} + \nabla \cdot \mathbf{F} + \sigma_a \phi = Q, \tag{1}$$

$$\mathbf{F} = -D\nabla\phi, \tag{2}$$

where t is the time variable, v is the particle speed (length/time), ϕ is the intensity (energy/area-time), $\mathbf{F}$ is the flux (energy/area-time), σ_a is the macroscopic absorption cross section (inverse length), Q is the source function (energy/volume-time), and D is the diffusion coefficient (length). Equations (1) and (2) constitute a first-order system for the flux and intensity. A diffusion equation for the intensity is obtained by using Eq. (2) to eliminate the flux from Eq. (1). However, it is convenient for our purposes to work with the first-order equations. Following Kershaw [1] and Pert [2], we assume a logically rectangular, quadrilateral $r-z$ mesh, having logical coordinates k and l. Each cell is assumed to be non-reentrant and homogeneous, but different cells may be composed of different materials. Although each cell is homogeneous, a variation of the diffusion coefficient is allowed within each cell to accomodate problems in which the diffusion coefficient can strongly vary within a homogeneous cell, e.g., radiative transfer problems. The logical coordinates and quadrant numbering for a single mesh cell are shown in Fig. 1. Intensities are defined at the cell center and at each cell edge, whereas fluxes are defined only at each cell edge.

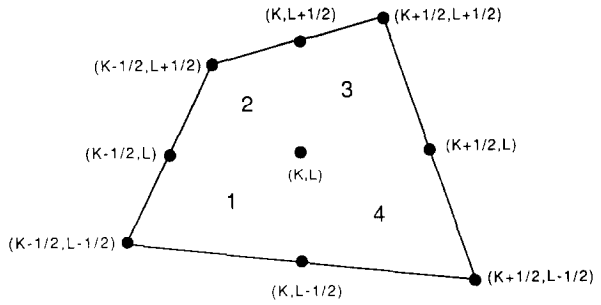

FIG. 1. Logical coordinates and quadrant numbering for an r-z quadrilateral cell on a logically rectangular mesh.

A diffusion coefficient is defined for each quadrant of the quadrilateral. In the derivation that follows we neglect considerations of material motion. It is reasonably straightforward to include the effects of material motion once the basic scheme has been defined. Differencing Eq. (1) fully implicitly in time, integrating over the cell volume shown in Fig. 1, and invoking the divergence theorem, we obtain a finite-difference expression for energy conservation within the cell,

$$\begin{aligned}\frac{1}{v}\frac{(\phi_{k,l}^{n+1}-\phi_{k,l}^{n})}{\Delta t}V_{k,l} &+ \mathbf{F}_{k+1/2,l}^{n+1}\cdot\mathbf{A}_{k+1/2,l} \\ &- \mathbf{F}_{k-1/2,l}^{n+1}\cdot\mathbf{A}_{k-1/2,l} \\ &+ \mathbf{F}_{k,l+1/2}^{n+1}\cdot\mathbf{A}_{k,l+1/2} - \mathbf{F}_{k,l-1/2}^{n+1}\cdot\mathbf{A}_{k,l-1/2} \\ &+ \sigma_{a,k,l}\phi_{k,l}^{n+1}V_{k,l} = Q_{k,l}V_{k,l},\end{aligned} \tag{3}$$

where n denotes the time index, Δt denotes the time step, $\mathbf{A}_{k+1/2,l}$ denotes a vector outwardly-directed from cell (k,l) and normal to the edge at $(k+1/2, l)$ with a magnitude equal to the area associated with that cell edge, $\mathbf{A}_{k,l+1/2}$ denotes a vector outwardly-directed from cell (k, l) and normal to the edge at $(k, l+\frac{1}{2})$ with a magnitude equal to the area associated with that cell edge, and $V_{k,l}$ denotes the cell volume. Explicit expressions for the geometric quantities appearing in Eq. (3) are

$$\begin{aligned}\mathbf{A}_{k+1/2,l} = 2\pi r_{k+1/2,l}[&\mathbf{r}(z_{k+1/2,l+1/2}-z_{k+1/2,l-1/2}) \\ &-\mathbf{z}(r_{k+1/2,l+1/2}-r_{k+1/2,l-1/2})],\end{aligned} \tag{4}$$

$$\begin{aligned}\mathbf{A}_{k,l+1/2} = 2\pi r_{k,l+1/2}[&\mathbf{r}(z_{k-1/2,l+1/2}-z_{k+1/2,l+1/2}) \\ &-\mathbf{z}(r_{k-1/2,l+1/2}-r_{k+1/2,l+1/2})],\end{aligned} \tag{5}$$

where $\mathbf{r}$ and $\mathbf{z}$ are unit vectors oriented along the r-coordinate and z-coordinate, respectively, and

$$V_{k,l} = \pi(\mathbf{r}_1 J_1 + \mathbf{r}_2 J_2), \tag{6}$$

where

$$\mathbf{r}_1 = \tfrac{1}{3}(r_{k+1/2,l-1/2} + r_{k-1/2,l-1/2} + r_{k-1/2,l+1/2}), \quad (7)$$

$$\mathbf{r}_2 = \tfrac{1}{3}(r_{k+1/2,l-1/2} + r_{k+1/2,l+1/2} + r_{k-1/2,l+1/2}), \quad (8)$$

$$\begin{aligned} J_1 = {} & (r_{k+1/2,l-1/2} - r_{k-1/2,l-1/2}) \\ & \times (z_{k-1/2,l+1/2} - z_{k-1/2,l-1/2}) \\ & - (r_{k-1/2,l+1/2} - r_{k-1/2,l-1/2}) \\ & \times (z_{k+1/2,l-1/2} - z_{k-1/2,l-1/2}), \end{aligned} \quad (9)$$

$$\begin{aligned} J_2 = {} & (r_{k+1/2,l+1/2} - r_{k-1/2,l+1/2}) \\ & \times (z_{k+1/2,l+1/2} - z_{k+1/2,l-1/2}) \\ & - (r_{k+1/2,l+1/2} - r_{k+1/2,l-1/2}) \\ & \times (z_{k+1/2,l+1/2} - z_{k-1/2,l+1/2}). \end{aligned} \quad (10)$$

Note that $\mathbf{A}_{k-1/2,l}$ and $\mathbf{A}_{k,l-1/2}$ are implicitly defined by Eqs. (4) and (5), respectively. The fluxes are eliminated from Eq. (3) by defining them in terms of the cell-center and cell-edge intensities. It is clear from Eq. (2) that a definition for the flux at a cell edge follows directly from a definition for the gradient of the intensity at that edge. The gradient of the intensity can be expressed in terms of partial derivatives with respect to the logical coordinates as follows: [1]

$$\nabla\phi = J^{-1}\left[\frac{\partial\phi}{\partial k}\left(\mathbf{r}\frac{\partial z}{\partial l} - \mathbf{z}\frac{\partial r}{\partial l}\right) - \frac{\partial\phi}{\partial l}\left(\mathbf{r}\frac{\partial z}{\partial k} - \mathbf{z}\frac{\partial r}{\partial k}\right)\right], \quad (11)$$

where the Jacobian of the transformation is given by:

$$J = \frac{\partial r}{\partial k}\frac{\partial z}{\partial l} - \frac{\partial r}{\partial l}\frac{\partial z}{\partial k}. \quad (12)$$

It is important to note that Eq. (11) is based upon the assumption that k and l form a right-handed coordinate system like r and z. Certain sign changes occur if this is not the case. Furthermore, this expression is only meaningful if the mapping between the logical and spatial coordinate systems is smooth. Although the mapping between the logical coordinates and the spatial coordinates is generally not smooth *across* cells, it is both smooth and linear *within* each cell. Thus as long as we take differences between intensities that either lie within or on the edge of a single cell, we can expect finite-difference approximations based upon Eq. (11) to become increasingly accurate as the cell size is reduced. Furthermore, because the mapping is *linear* within each cell, we can expect such approximations to be *exact* for linear functions of r and z. By restricting the gradient expressions so that differences are never taken across cell boundaries, we accomodate the possibility of material discontinuities at the cell interfaces, however, this also forces us to introduce two definitions for each cell-edge flux: one for each of the two cells that share each edge.

Three distinct intensity values are needed to construct a gradient according to Eq. (11). Thus, following Fig. 1, we can associate a gradient with each quadrant of the quadrilateral. Since we also associate each quadrant with a diffusion coefficient, it follows from Eq. (2) that we can associate each quadrant with a flux. The quadrant fluxes are defined as follows:

$$\mathbf{F}^{(1)}_{k,l} = -\frac{2D^{(1)}_{k,l}}{J_{k,l}}\left[(\phi_{k,l} - \phi_{k-1/2,l})\,\zeta_{k,l} - (\phi_{k,l} - \phi_{k,l-1/2})\,\eta_{k,l}\right], \quad (13)$$

$$\mathbf{F}^{(2)}_{k,l} = -\frac{2D^{(2)}_{k,l}}{J_{k,l}}\left[(\phi_{k,l} - \phi_{k-1/2,l})\,\zeta_{k,l} - (\phi_{k,l+1/2} - \phi_{k,l})\,\eta_{k,l}\right], \quad (14)$$

$$\mathbf{F}^{(3)}_{k,l} = -\frac{2D^{(3)}_{k,l}}{J_{k,l}}\left[(\phi_{k+1/2,l} - \phi_{k,l})\,\zeta_{k,l} - (\phi_{k,l+1/2} - \phi_{k,l})\,\eta_{k,l}\right], \quad (15)$$

$$\mathbf{F}^{(4)}_{k,l} = -\frac{2D^{(4)}_{k,l}}{J_{k,l}}\left[(\phi_{k+1/2,l} - \phi_{k,l})\,\zeta_{k,l} - (\phi_{k,l} - \phi_{k,l-1/2})\,\eta_{k,l}\right], \quad (16)$$

where, following Fig. 1, $\mathbf{F}^{(i)}_{k,l}$ and $D^{(i)}_{k,l}$ are the respective flux and diffusion coefficient associated with the ith quadrant in cell (k, l), and where

$$\zeta_{k,l} = \mathbf{r}(z_{k,l+1/2} - z_{k,l-1/2}) - \mathbf{z}(r_{k,l+1/2} - r_{k,l-1/2}), \quad (17)$$

$$\eta_{k,l} = \mathbf{r}(z_{k+1/2,l} - z_{k-1/2,l}) - \mathbf{z}(r_{k+1/2,l} - r_{k-1/2,l}), \quad (18)$$

and where

$$\begin{aligned} J_{k,l} = {} & (r_{k+1/2,l} - r_{k-1/2,l})(z_{k,l+1/2} - z_{k,l-1/2}) \\ & - (r_{k,l+1/2} - r_{k,l-1/2})(z_{k+1/2,l} - z_{k-1/2,l}). \end{aligned} \quad (19)$$

The cell-edge fluxes are defined in terms of the quadrant fluxes as follows:

$$\mathbf{F}^{-}_{k+1/2,l} = (\mathbf{F}^{(3)}_{k,l} + \mathbf{F}^{(4)}_{k,l})/2, \quad (20)$$

$$\mathbf{F}^{+}_{k-1/2,l} = (\mathbf{F}^{(1)}_{k,l} + \mathbf{F}^{(2)}_{k,l})/2, \quad (21)$$

$$\mathbf{F}^{-}_{k,l+1/2} = (\mathbf{F}^{(2)}_{k,l} + \mathbf{F}^{(3)}_{k,l})/2, \quad (22)$$

$$\mathbf{F}^{+}_{k,l-1/2} = (\mathbf{F}^{(1)}_{k,l} + \mathbf{F}^{(4)}_{k,l})/2, \quad (23)$$

where the superscripts "+" and "−" associate each cell-edge flux with a particular cell in that the flux is defined in terms of intensities that either lie on the edge or at the center of that cell. For instance, $\mathbf{F}^{-}_{k+1/2,l}$ and $\mathbf{F}^{+}_{k+1/2,l}$ are both defined at edge $(k+\frac{1}{2}, l)$, but $\mathbf{F}^{-}_{k+1/2,l}$ is associated with cell (k, l) and is explicitly defined by Eq. (20), whereas $\mathbf{F}^{+}_{k+1/2,l}$ is associated with cell $(k+1, l)$ and is implicitly defined by

Eq. (21). Taking these dual flux definitions into account, Eq. 3 is rewritten as follows:

$$\frac{1}{v}\frac{(\phi_{k,l}^{n+1}-\phi_{k,l}^{n})}{\Delta t}V_{k,l}+\mathbf{F}_{k+1/2,l}^{-}\cdot\mathbf{A}_{k+1/2,l}-\mathbf{F}_{k-1/2,l}^{+}\cdot\mathbf{A}_{k-1/2,l}$$
$$+\mathbf{F}_{k,l+1/2}^{-}\cdot\mathbf{A}_{k,l+1/2}-\mathbf{F}_{k,l-1/2}^{+}\cdot\mathbf{A}_{k,l-1/2}$$
$$+\sigma_{a,k,l}\phi_{k,l}^{n+1}V_{k,l}=Q_{k,l}V_{k,l}. \tag{24}$$

Note that all of the fluxes appearing in Eq. (24) are associated with cell (k, l) and are explicitly defined by Eqs. (20) through (23).

Having defined two fluxes at each cell face, we next require that the flux component normal to each face be continuous:

$$\mathbf{F}_{k+1/2,l}^{-}\cdot\mathbf{N}_{k+1/2,l}=\mathbf{F}_{k+1/2,l}^{+}\cdot\mathbf{N}_{k+1/2,l}, \tag{25}$$

$$\mathbf{F}_{k,l+1/2}^{-}\cdot\mathbf{N}_{k,l+1/2}=\mathbf{F}_{k,l+1/2}^{+}\cdot\mathbf{N}_{k,l+1/2}, \tag{26}$$

where

$$\mathbf{N}=\frac{\mathbf{A}}{\|\mathbf{A}\|}. \tag{27}$$

This continuity-of-flux requirement achieves two important results: first it uniquely defines the net rate of energy flow across each cell-edge, and second it gives the exact interface boundary condition if a material discontinuity exists at a cell edge. Unique flow rates are essential because they ensure global energy conservation. For instance, if we sum Eq. (24) over any connected set of cells, we find that the two flow terms associated with each interior cell edge cancel one other because of the flux-continuity conditions. This cancellation process leads to a finite-difference analogue of the divergence theorem, and hence to global energy conservation. At a material interface, the component of the flux normal to the interface must be continuous, but tangential components may be discontinuous. Thus our flux continuity requirement results in a rigorous treatment of material discontinuities in the sense that the exact boundary condition is met at material interfaces.

Equations (20) through (23) are used to eliminate the fluxes from Eqs. (24), (25), and (26), and obtain a system of equations for the cell-center and cell-edge intensities. Equation (24) is an energy conservation equation associated with each cell-center that produces the five-point coupling illustrated in Fig. 2. Equation (25) is a flux-continuity equation associated with each k-edge that produces the seven-point coupling illustrated in Fig. 3. Equation (26) is a flux-continuity equation associated with each l-edge that produces a seven-point coupling analogous to that for k-edges. We have defined one equation for each of the unknowns, so our derivation of the difference equations for cells on the interior of the mesh is complete.

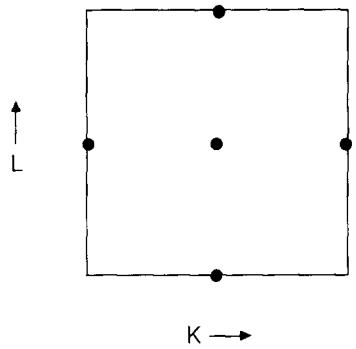

FIG. 2. Stencil for cell-center conservation equations.

We now consider boundary conditions for our method. At cell edges on the outer boundary of the mesh, the flux continuity condition is replaced with one of the following extrapolated-endpoint boundary conditions:

$$\phi_{K+1/2,l}-[\mathbf{F}_{K+1/2,l}^{-}\cdot\mathbf{N}_{K+1/2,l}]\,\delta_r=\phi_{K+1/2,l}^{b}, \tag{28}$$

$$\phi_{1/2,l}+[\mathbf{F}_{1/2,l}^{+}\cdot\mathbf{N}_{1/2,l}]\,\delta_r=\phi_{1/2,l}^{b}, \tag{29}$$

$$\phi_{k,L+1/2}-[\mathbf{F}_{k,L+1/2}^{-}\cdot\mathbf{N}_{k,L+1/2}]\,\delta_r=\phi_{k,L+1/2}^{b}, \tag{30}$$

$$\phi_{k,1/2}+[\mathbf{F}_{k,1/2}^{+}\cdot\mathbf{N}_{k,1/2}]\,\delta_r=\phi_{k,1/2}^{b}, \tag{31}$$

where K and L denote the maximum values of k and l, respectively, ϕ^b denotes the extrapolated intensity value, and δ_r denotes a relative extrapolation length defined with respect to the diffusion coefficient, i.e., the absolute extrapolation length is equal to $\delta_r D$. Note that for a Marshak boundary condition, $\delta_r=2$, and for a Mark boundary condition, $\delta_r=\sqrt{3}$. As can be seen from the spatial indexing, Eqs. (28) through (31) respectively correspond to the four types of boundaries on a logically rectangular mesh.

Our method represents a straightforward generalization to the non-orthogonal case of the standard five-point orthogonal-mesh scheme. If the mesh is orthogonal, the seven-point flux-continuity coupling in our scheme reduces to three-point coupling between each edge intensity and the two adjacent cell-center intensities. With this reduced

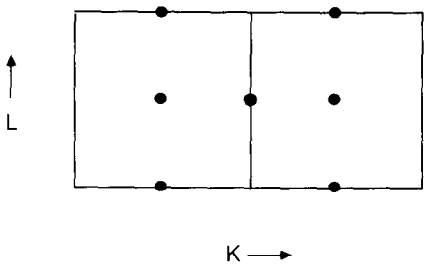

FIG. 3. Stencil for k-edge flux-continuity equations.

coupling, the edge intensities can be explicitly eliminated to obtain the standard five-point cell-center scheme. If the mesh is non-orthogonal, the cell-edge intensities cannot be explicitly eliminated and the diffusion matrix is generally assymmetric. In addition, certain of the off-diagonal matrix elements are of the same sign as their corresponding diagonal elements. Thus, as is the case for the Kershaw [1] and Pert [2] schemes, positivity of the solution cannot be guaranteed.

3. MESH DISTORTIONS

The condition of our diffusion matrix is no more sensitive to simple skewing of the mesh than standard schemes, but unlike standard schemes, it is quite sensitive to certain types of "hourglass" cell distortions. Before we can proceed with a discussion of the effects of such distortions, we must give both qualitative and quantitative definitions for mesh "hourglassing".

Qualitatively, hourglassing is the extent to which a quadrilateral departs from a parallelogram. For instance, a quadrilateral and its associated parallelogram are shown in Fig. 4. If this quadrilateral were not hourglassed, the parallelogram and quadrilateral would be identical. There are many possible definitions for hourglassing. We give one that is particularly convenient for our purposes. A measure of the hourglassing associated with cell (k, l) is

$$H_{k,l} = H_{k,l}^{(k,-)} + H_{k,l}^{(k,+)} + H_{k,l}^{(l,-)} + H_{k,l}^{(l,+)}, \tag{32}$$

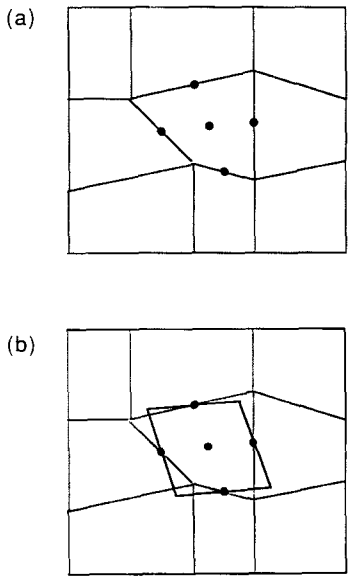

FIG. 4. Hourglassed quadrilateral (a) and associated parallelogram (b).

where

$$H_{k,l}^{(k,-)} = 1 - \frac{\Delta\mathbf{R}_{k,l-1/2}^{k} \cdot \Delta\mathbf{R}_{k,l}^{k}}{\|\Delta\mathbf{R}_{k,l-1/2}^{k}\| \, \|\Delta\mathbf{R}_{k,l}^{k}\|}, \tag{33}$$

$$H_{k,l}^{(k,+)} = 1 - \frac{\Delta\mathbf{R}_{k,l+1/2}^{k} \cdot \Delta\mathbf{R}_{k,l}^{k}}{\|\Delta\mathbf{R}_{k,l+1/2}^{k}\| \, \|\Delta\mathbf{R}_{k,l}^{k}\|}, \tag{34}$$

$$H_{k,l}^{(l,-)} = 1 - \frac{\Delta\mathbf{R}_{k-1/2,l}^{l} \cdot \Delta\mathbf{R}_{k,l}^{l}}{\|\Delta\mathbf{R}_{k-1/2,l}^{l}\| \, \|\Delta\mathbf{R}_{k,l}^{l}\|}, \tag{35}$$

$$H_{k,l}^{(l,+)} = 1 - \frac{\Delta\mathbf{R}_{k+1/2,l}^{l} \cdot \Delta\mathbf{R}_{k,l}^{l}}{\|\Delta\mathbf{R}_{k+1/2,l}^{l}\| \, \|\Delta\mathbf{R}_{k,l}^{l}\|}, \tag{36}$$

where the k-difference cell-edge and cell-center vectors are respectively given by

$$\Delta\mathbf{R}_{k,l\pm1/2}^{k} = \mathbf{R}_{k+1/2,l\pm1/2} - \mathbf{R}_{k-1/2,l\pm1/2}, \tag{37}$$

$$\Delta\mathbf{R}_{k,l}^{k} = \mathbf{R}_{k+1/2,l} - \mathbf{R}_{k-1/2,l}, \tag{38}$$

and the l-difference cell-edge and cell-center vectors are respectively given by

$$\Delta\mathbf{R}_{k\pm1/2,l}^{l} = \mathbf{R}_{k\pm1/2,l+1/2} - \mathbf{R}_{k\pm1/2,l-1/2}, \tag{39}$$

$$\Delta\mathbf{R}_{k,l}^{l} = \mathbf{R}_{k,l+1/2} - \mathbf{R}_{k,l-1/2}, \tag{40}$$

and $\mathbf{R}_{k,l}$ denotes the standard position vector, $(r_{k,l}, z_{k,l})$. We refer to $H_{k,l}$ as the total hourglassing measure for cell (k, l), and we refer to $H_{k,l}^{(k,-)}$, $H_{k,l}^{(k,+)}$, $H_{k,l}^{(l,-)}$, and $H_{k,l}^{(l,+)}$ as the partial hourglassing measures for cell (k, l). The k-difference vectors defined by Eqs. (37) and (38) are illustrated in Fig. 5. The l-difference vectors are analogously defined. Our measure of hourglassing is based upon the following facts. A quadrilateral is a parallelogram if and only if all three k-difference vectors are parallel to one another and all three l-difference vectors are parallel to one another. Since the cosine of the angle between two vectors is unity if and only if they are parallel, we can measure hourglassing in terms of dot products between the k-difference vectors and l-difference vectors. Note from Eqs. (32) through (36) that $H_{k,l}$ is constructed from these dot products in such a way

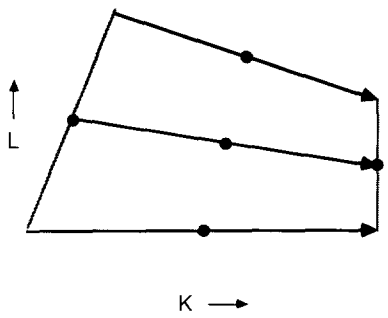

FIG. 5. k-difference vectors for a quadrilateral.

that a parallelogram gives a value of zero and a quadrilateral that is not a parallelogram gives a positive non-zero value. In particular, the total measure is the sum of the partial measures, and each partial measure, which is associated with a particular dot product, gives values from zero to two.

If there is no hourglassing of the mesh in $x-y$ geometry, our diffusion matrix is symmetric and positive-definite. Under the same conditions, asymmetries persist in $r-z$ geometry, but these are rather weak and do not result in significant ill-conditioning of the diffusion matrix. On the other hand, severe hourglassing of the mesh can cause our diffusion matrix to become highly asymmetric and highly ill-conditioned. In particular, if a cell-edge difference vector is perpendicular to the corresponding cell-center difference vector, the flux at that edge does not depend upon the intensity at that edge. This is clearly non-physical and leads to ill-conditioning of the diffusion matrix. An example of such a cell is given in Fig. 6. Furthermore, if the angle between a cell-edge difference vector and its associated cell-center difference vector is greater than 90°, a non-physical relationship between the edge intensity and flux is obtained, which also can lead to ill-conditioning of the diffusion matrix.

Fortunately, we have found that this type and severity of hourglassing is generally quite rare in production calculations. In particular, such cells appear with about the same frequency as bowtie and boomerang cells. If a large number of such cells appear in a calculation, one should obviously rezone the mesh. However, in many instances, a small number of such cells appear in regions of the problem that are not very important. In this situation it is desirable to be able to continue the calculation without rezoning the mesh. We have developed a "fixup" procedure for our differencing scheme which allows us to do this as long as all of the cells have a positive volume. To our knowledge, all Lagrangian hydrodynamics algorithms require a mesh rezoning when a cell with a negative volume appears. Thus if the hydrodynamics calculation can continue without rezoning, our diffusion calculation can also continue.

The fixup procedure is quite simple. Since severe hourglassing of a quadrilateral causes the ill-conditioning, we simply replace the quadrilateral with its associated parallelogram, as illustrated in Fig. 4. Note that the locations of the unknowns remain invariant under this substitution. Also note that the cell-edge area vectors become doubly defined. For instance, the adjacent parallelogram and quadrilateral cells shown in Fig. 4 do not share an entire edge, but rather share only a single point (the point at which the edge intensity is defined). Thus if we consider a hybrid quadrilateral/parallelogram mesh, there are *two* area vectors associated with each cell-edge point: one associated with each of the cells that share that point. To accomodate this situation, we add a superscript to the notation for the cell-edge area vectors that is analogous to that defined for the cell-edge fluxes. In particular, $\mathbf{A}^{+}_{k-1/2,l}$, $\mathbf{A}^{-}_{k+1/2,l}$, $\mathbf{A}^{+}_{k,l-1/2}$, and $\mathbf{A}^{-}_{k,l+1/2}$ denote the area vectors associated with cell (k, l), and are analogous to $\mathbf{F}^{+}_{k-1/2,l}$, $\mathbf{F}^{-}_{k+1/2,l}$, $\mathbf{F}^{+}_{k,l-1/2}$, and $\mathbf{F}^{-}_{k,l+1/2}$, respectively.

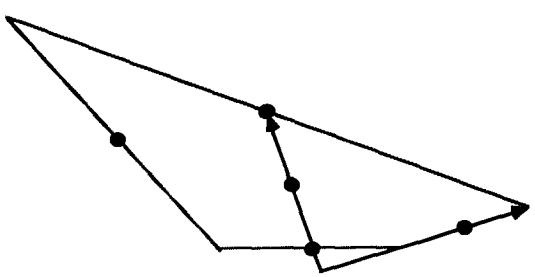

FIG. 6. Hourglassed configuration leading to an ill-conditioned diffusion matrix.

The cell-center equation for the parallelogram is obtained by first performing the standard integration of the diffusion equation over the parallelogram cell, and then substituting the quadrilateral volume for the parallelogram volume. In particular, Eq. (24) is generalized to accomodate both the basic and fixup schemes as

$$\begin{aligned}\frac{1}{v}\frac{(\phi^{n+1}_{k,l}-\phi^{n}_{k,l})}{\Delta t}V_{k,l}&+\mathbf{F}^{-}_{k+1/2,l}\cdot\mathbf{A}^{-}_{k+1/2,l}\\&-\mathbf{F}^{+}_{k-1/2,l}\cdot\mathbf{A}^{+}_{k-1/2,l}\\&+\mathbf{F}^{-}_{k,l+1/2}\cdot\mathbf{A}^{-}_{k,l+1/2}-\mathbf{F}^{+}_{k,l-1/2}\cdot\mathbf{A}^{+}_{k,l-1/2}\\&+\sigma_{a,k,l}\phi^{n+1}_{k,l}V_{k,l}=Q_{k,l}V_{k,l},\end{aligned}\tag{41}$$

where the parallelogram cell-edge area vectors replace the quadrilateral cell-edge area vectors when the fixup is used. Note that the expressions for the cell-edge fluxes, Eqs. (20) through (23), and the equations for the quadrant fluxes, Eqs. (13) through (16) remain invariant under the parallelogram fixup. This is so because the positions of the unknowns remain invariant and the Jacobian of a quadrilateral and its associated parallelogram are always identical.

The cell-edge equations are obtained with a simple generalization of the standard flux-continuity equations. In particular, rather than require continuity of the flux component normal to each cell edge, we require that the net energy flow between adjacent cells be uniquely defined. On a standard quadrilateral mesh, these two conditions are equivalent, but they are not necessarily equivalent when a quadrilateral is replaced with a parallelogram. The standard flux-continuity equations, Eqs. (25) and (26), are generalized as

$$\mathbf{F}^{-}_{k+1/2,l}\cdot\mathbf{A}^{-}_{k+1/2,l}=\mathbf{F}^{+}_{k+1/2,l}\cdot\mathbf{A}^{+}_{k+1/2,l},\tag{42}$$

$$\mathbf{F}^{-}_{k,l+1/2}\cdot\mathbf{A}^{-}_{k,l+1/2}=\mathbf{F}^{+}_{k,l+1/2}\cdot\mathbf{A}^{+}_{k,l+1/2},\tag{43}$$

where the parallelogram cell-edge area vectors replace the quadrilateral cell-edge area vectors when the fixup is used. If cells adjacent to an edge are quadrilateral cells, the two area vectors defined for that edge are identical, and Eqs. (42) and (43) become equivalent to the original flux-continuity equations. If one or both of the adjacent cells is a parallelogram, Eqs. (42) and (43) ensure a unique energy flow rate between the cells and, hence, ensure energy conservation.

As one would expect, the extrapolated-endpoint boundary conditions, Eqs. (28) through (31), are generalized simply by substituting the doubly-defined cell-edge area vectors for the standard vectors,

$$\phi_{K+1/2,l} - [\mathbf{F}^{-}_{K+1/2,l} \cdot \mathbf{N}^{-}_{K+1/2,l}]\, \delta_r = \phi^b_{K+1/2,l}, \quad (44)$$

$$\phi_{1/2,l} + [\mathbf{F}^{+}_{1/2,l} \cdot \mathbf{N}^{+}_{1/2,l}]\, \delta_r = \phi^b_{1/2,l}, \quad (45)$$

$$\phi_{k,L+1/2} - [\mathbf{F}^{-}_{k,L+1/2} \cdot \mathbf{N}^{-}_{k,L+1/2}]\, \delta_r = \phi^b_{k,L+1/2}, \quad (46)$$

$$\phi_{k,1/2} + [\mathbf{F}^{+}_{k,1/2} \cdot \mathbf{N}^{+}_{k,1/2}]\, \delta_r = \phi^b_{k,1/2}, \quad (47)$$

where

$$\mathbf{N}^{\pm} = \mathbf{A}^{\pm}/\|\mathbf{A}^{\pm}\| \quad (48)$$

and where the parallelogram cell-edge vectors replace the quadrilateral cell-edge area vectors when the fixup is used.

The parallelogram fixup scheme preserves the constant homogeneous solution and gives both local and global energy conservation, but does not preserve linear homogeneous solutions. It is not as accurate as the basic scheme, but is nonetheless quire accurate relative to standard schemes such as Kershaw's scheme. This is no doubt due to the fact that if one employs the parallelogram fixup in *all* cells, one obtains a scheme that is nearly identical to a certain variational scheme. This variational scheme is described elsewhere [4].

The fixup procedure is invoked for the following types of cells:

1. Boomerang cells.
2. Bowtie cells.
3. Cells for which any one of the component hourglassing functions (Eqs. (33) through (36)) gives a value greater than 0.1.

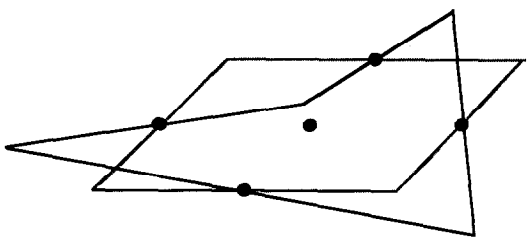

FIG. 7. Boomerang cell and associated parallelogram.

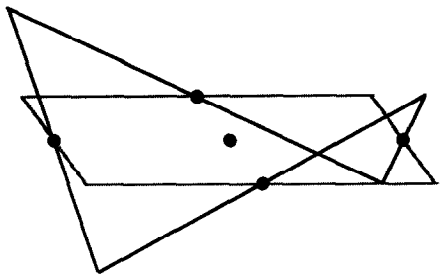

FIG. 8. Bowtie cell and associated parallelogram.

A boomerang cell and a bowtie cell and their associated parallelograms are shown in Figs. 7 and 8. It can be seen that the parallelograms are well defined even though the boomerang cell is re-entrant and the bowtie cell has a region of negative volume. If the net volume of the bowtie cell is negative, the parallelogram will not be well defined and a rezoning of the mesh is required to continue.

In closing this section we review the generalized equations, which accommodate both the basic diffusion scheme and the parallelogram fixup scheme. The cell-edge fluxes are defined by Eqs. (20) through (23). The energy balance equation, Eq. (41), applies at cell centers, and the continuity-of-flow equations, Eqs. (42) and (43), apply at interior cell edges. The extrapolated-endpoint intensity equations, Eqs. (44) through (47), apply at the boundary edges. Note that the only effect of the parallelogram fixup is to substitute the parallelogram cell-edge area vectors into these equations in place of the quadrilateral cell-edge area vectors. Thus the fixup is achieved entirely through geometry definitions. This is very straightforward and does not generate significant overhead.

4. SOLUTION OF THE EQUATIONS

We have developed both a simple line-relaxation method and an associated multigrid method to solve our equations. We first discuss the line relaxation method, and then discuss the multigrid method.

4.1. *The Line Relaxation Method*

Our line relaxation method is analogous to the line relaxation method used with the standard five-point orthogonal-mesh diffusion scheme [5]. Therefore we shall only briefly describe it. There are two types of line solutions associated with an iteration: k-line solutions and l-line solutions. In a k-line solution, one simultaneously solves for all of the unknowns associated with a fixed value of l, while holding all of the remaining unknowns fixed. The unknowns associated with such a solution are shown in Fig. 9. The unknowns associated with an l-line solution are

$$\mathbf{F}^{+}_{k-1/2,l} = -\frac{(D^{(1)}_{k,l} + D^{(2)}_{k,l})}{J_{k,l}} (\phi_{k,l} - \phi_{k-1/2,l})\, \zeta_{k,l}, \quad (57)$$

$$\mathbf{F}^{-}_{k,l+1/2} = \frac{(D^{(2)}_{k,l} + D^{(3)}_{k,l})}{J_{k,l}} (\phi_{k,l+1/2} - \phi_{k,l})\, \eta_{k,l}, \quad (58)$$

$$\mathbf{F}^{+}_{k,l-1/2} = \frac{(D^{(1)}_{k,l} + D^{(4)}_{k,l})}{J_{k,l}} (\phi_{k,l} - \phi_{k,l-1/2})\, \eta_{k,l}. \quad (59)$$

Under these definitions, the continuity-of-flow equations are reduced from seven-point equations to three-point equations, each involving only the corresponding cell-edge intensity, the two adjacent cell-center intensities, and the cell-edge component of the residual vector. This enables the cell-edge intensities to be explicitly eliminated from the equations, with the result that a symmetric, positive-definite, five-point, cell-centered diffusion equation is obtained. When the mesh is orthogonal, this equation is equivalent to both the standard five-point scheme and our generalized scheme. Thus Eq. (55) is actually exact when the mesh is orthogonal.

The fourth step in our multigrid method is to use a "black-box" multigrid scheme, previously developed by Dendy [6] to *approximately* solve Eq. (55). In particular, we accept the solution obtained from a single blackbox multigrid iteration.

In more detail, following Eqs. (56) through (59) and suppressing the $m + 1/3$ on $\tilde{\varepsilon}$, we can write

$$bk^1_{k+1/2,l}\tilde{\varepsilon}_{k,l} + bk^2_{k+1/2,l}\tilde{\varepsilon}_{k+1/2,l} + bk^3_{k+1/2,l}\tilde{\varepsilon}_{k+1,l} = R^{m+1/3}_{k+1/2,l} \quad (60)$$

$$bl^1_{k,l+1/2}\tilde{\varepsilon}_{k,l} + bl^2_{k,l+1/2}\tilde{\varepsilon}_{k,l+1/2} + bl^3_{k,l+1/2}\tilde{\varepsilon}_{k,l+1} = R^{m+1/3}_{k,l+1/2}, \quad (61)$$

where $bk^1_{k+1/2,l}$, $bk^2_{k+1/2,l}$, and $bk^3_{k+1/2,l}$ denote the coefficients of the k-edge equations and where $bl^1_{k,l+1/2}$, $bl^2_{k,l+1/2}$, and $bl^3_{k,l+1/2}$ denote the coefficients of the l-edge equations. Similarly, using $bc^1_{k,l}$, ..., $bc^5_{k,l}$ as the coefficients for the cell-center equations, we write

$$bc^1_{k,l}\tilde{\varepsilon}_{k-1/2,l} + bc^2_{k,l}\tilde{\varepsilon}_{k,l-1/2} + bc^3_{k,l}\phi_{k,l} + bc^4_{k,l}\tilde{\varepsilon}_{k,l+1/2} + bc^5_{k,l}\tilde{\varepsilon}_{k+1/2,l} = R^{m+1/3}_{k,l}, \quad (62)$$

We use Eqs. (60) and (61) to solve for the edge $\tilde{\varepsilon}$'s in terms of the cell-center $\tilde{\varepsilon}$'s and substitute into Eq. (62). The result is

$$C\tilde{\varepsilon}_{k,l} = \mathbf{S}_{k,l}, \quad (63)$$

where

$$S_{k,l} = R^{m+1/3}_{k,l} - \frac{bc^4_{k,l}R^{m+1/3}_{k,l+1/2}}{bl^2_{k,l+1/2}} - \frac{bc^5_{k,l}R^{m+1/3}_{k+1/2,l}}{bk^2_{k+1/2,l}} - \frac{bc^2_{k,l}R^{m+1/3}_{k,l-1/2}}{bl^2_{k,l-1/2}} - \frac{bc^1_{k,l}R^{m+1/3}_{k-1/2,l}}{bk^2_{k-1/2,l}}, \quad (64)$$

and where C is a symmetric five-point difference operator on the cell-center $\tilde{\varepsilon}$'s i.e., on the $\tilde{\varepsilon}_{k,l}$'s. Equation (63) is solved approximately with one V-cycle of black box multigrid—discussed below—and the approximate solution—denoted as $\tilde{\varepsilon}^{m+1/3}_{k,l}$—is used as an additive correction:

$$\phi^{m+2/3}_{k,l} = \phi^{m+1/3}_{k,l} + \tilde{\varepsilon}^{m+1/3}_{k,l}, \quad (65)$$

$$\phi^{m+2/3}_{k+1/2,l} = \phi^{m+1/3}_{k+1/2,l} + \left(\frac{-bk^3_{k+1/2,l}\tilde{\varepsilon}^{m+1/3}_{k+1,l} - bk^1_{k+1/2,l}\tilde{\varepsilon}^{m+1/3}_{k,l} + R^{m+1/3}_{k+1/2,l}}{bk^2_{k+1/2,l}}\right),$$

$$\phi^{m+2/3}_{k,l+1/2} = \phi^{m+1/3}_{k,l+1/2} + \left(\frac{-bl^3_{k,l+1/2}\tilde{\varepsilon}^{m+1/3}_{k,l+1} - bl^1_{k,l+1/2}\tilde{\varepsilon}^{m+1/3}_{k,l} + R^{m+1/3}_{k,l+1/2}}{bl^2_{k,l+1/2}}\right). \quad (66), (67)$$

The fifth and final step in our multigrid method is to perform another line-relaxation iteration:

$$\boldsymbol{\phi}^{m+1} = A^{-1}B\boldsymbol{\phi}^{m+2/3} + A^{-1}\mathbf{Q}. \quad (68)$$

This is done to attenuate any high-frequency errors that may have been introduced into the solution in the fourth step. The simplified diffusion scheme can always be expected to reduce low-frequency errors, but if the mesh is highly skewed, it can actually *increase* the high-frequency errors. In severe cases, it is conceivable that one might need to perform more than one line-relaxation iteration in each of the first and last steps. However, we have not yet encountered a case where this was necessary.

In the black box multigrid method [6], the user provides a difference equation, such as Eq. (63), on a given grid, and the code automatically generates the auxiliary coarser grids and their corresponding operators. The black box multigrid method was specifically designed with equations like (63) in mind, that is, five-point or nine-point difference operators resulting from the discretization of problems with diffusion-coefficients jumping by orders of magnitude across internal interfaces. The method allows a number of choices for relaxation. In this case, because of the possible presence of high-aspect-ratio cells, the relaxation method chosen is red-black line relaxation by lines in k, followed by red–black line relaxation by lines in l. Since the residual $\mathbf{R}^{m+1/3}$

changes after every relaxation of the full set of equations, there is no point in solving Eq. (63) to great precision. Hence, only one V-cycle is used to solve it approximately.

The V-cycle used here consists of the following: one relaxation on G^M, the finest grid; projection of the residual [illegible]; etc., until the coarsest grid G^1 is reached; a direct solve on G^1; interpolation of the solution on G^1 to the next finer grid G^2 as an additive correction to the current solution on G^2; one relaxation sweep on G^2, etc. until G^M is reached; and finally another relaxation sweep on G^M before the step denoted by (65)–(67) is performed.

Further details of the black box multigrid method may be found in [7, 8]. In particular the defect correction idea performed here is a special case of the—admittedly nongeneral—procedure suggested in [7] for extending the black box multigrid method to systems of equations on staggered grids.

If we were too obsessed with multigrid methdology, it would be possible to be unhappy with the multigrid method used here. A more honest multigrid method, it could be argued, would carry the whole system of equations to the coarser grids. The usual way of treating systems of equations on staggered grids is to coarsen by cells [9], but it is unknown how to do this when the grids are distorted and when there are discontinuities of orders of magnitude present. Such difficulties were part of the motivation for the method arrived at in [7]. Even if one knew how to formulate a standard multigrid method for our diffusion scheme, it is not clear that such a method would be more efficient than our defect method. The cost of doing coarse-grid relaxations with the full system of equations would be far more than that associated with our simplified cell-center diffusion operator. Thus, to be competitive, a pure multigrid method might have to have significantly better convergence factors than our defect multigrid method.

Ninety percent of the execution time associated with one V-cycle of our multigrid method is spent performing the two fine-grid relaxation iterations. Thus the overhead of our multigrid method relative to relaxation alone is only about 10%. This exceptionally small overhead results from the relative simplicity of the coarse-grid equations.

5. COMPUTATIONAL RESULTS

In this section we present computational results relating to the accuracy and cost of our diffusion scheme. All calculations were performed on a CRAY-YMP computer. In all cases we compare our scheme with the Kershaw scheme because it is quite representative of existing cell-centered Lagrangian-mesh diffusion schemes. One would expect the same basic behavior from other schemes such as that of Pert [2].

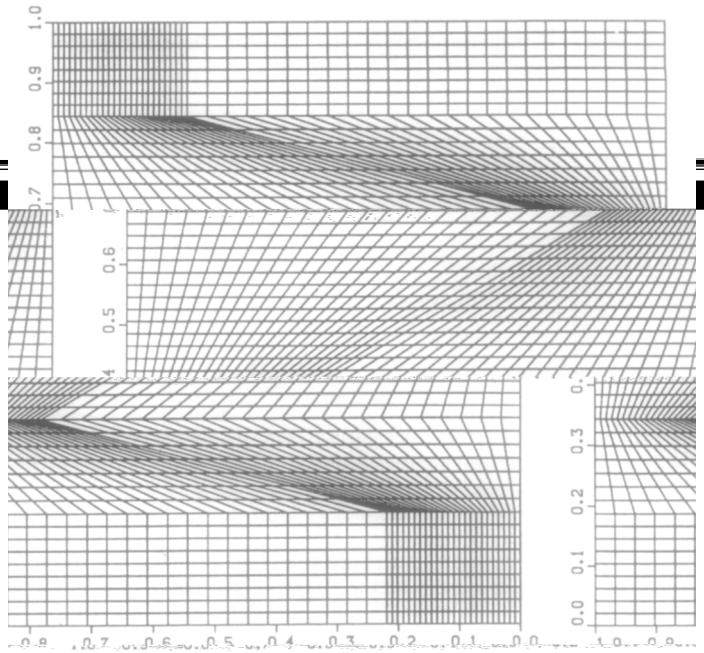

FIG. 10. The Kershaw "z-mesh."

5.1 *Accuracy*

In this section we first consider a simple 1D wave-propagation problem that is defined as

$$\frac{1}{v}\frac{\partial \phi}{\partial t} - \frac{\partial}{\partial z}\left[D\frac{\partial \phi}{\partial z}\right] = 0 \tag{69}$$

for $z \in [0, 1]$, with an extrapolated zero intensity at $z = -2D$ and an extrapolated unit intensity at $z = 1 + 2D$, where $v = 300$ and $D = \frac{1}{30}$. This one-dimensional problem is solved on a two-dimensional mesh by imposing reflective conditions along the top ($r = 1$) and bottom ($r = 0$) edges of the mesh. The steady state solution to this problem is given by

$$\phi = \frac{z + 2D}{1 + 4D}. \tag{70}$$

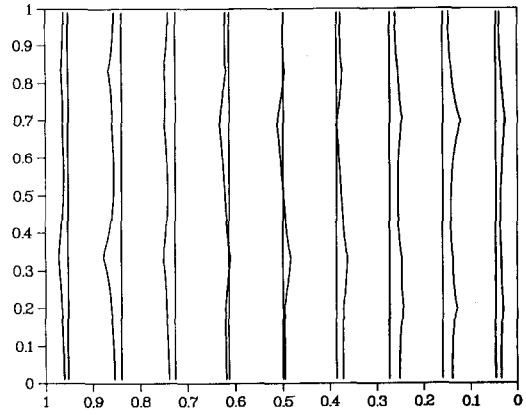

FIG. 11. Comparison of the steady-state contour solution for the wave propogation problem on the "z-mesh" using Kershaw's method with the exact solution.

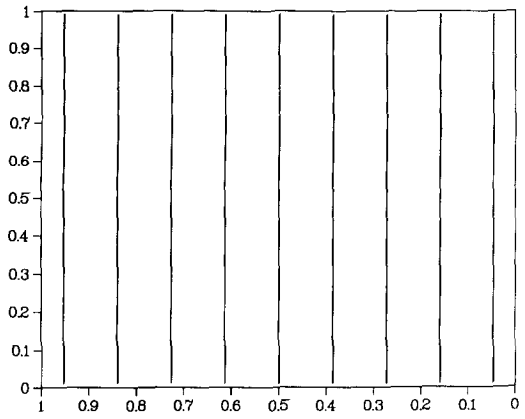

FIG. 12. Comparison of the steady-state contour solution for the wave propogation problem on the "z-mesh" using the new method with the exact solution.

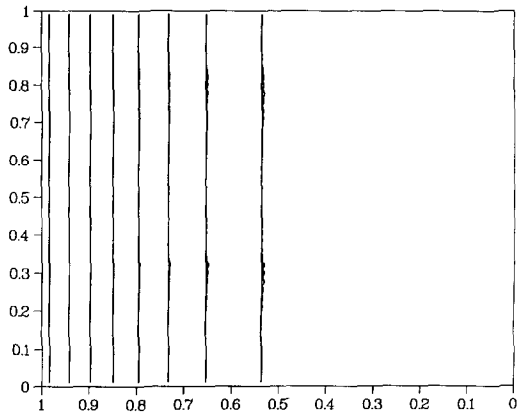

FIG. 14. Comparison of the early-time contour solution for the wave propogation problem on the "z-mesh" using the new method with the orthogonal mesh solution.

We first solved this problem on a mesh that was introduced by Kershaw [1], and it is shown in Fig. 10. There are 48 intervals each in k and l. Note that the derivatives of the coordinate mapping are discontinuous along four horizontal lines. Also note that the mesh is highly skewed, but there is very little hourglassing. As one would expect, the parallelogram fixup associated with out method is not invoked for this problem. The steady state contour solutions for this problem using Kershaw's method and our method are compared with the exact solution in Figs. 11 and 12, respectively. Note that our method gives the exact solution for this problem, while Kershaw's method gives a solution that follows the distorted mesh to some extent. Our method is exact for this problem because the solution is linear in z and constant in r. Contour solutions at $t = 0.001$ obtained with Kershaw's method and our method are compared with a 48×48 orthogonal mesh solution in Figs. 13 and 14, respectively. The dynamic solution at early times is not linear in z, but rather is exponential in z. Our scheme is not exact for such solutions; thus our scheme does exhibit some distortion, but it is very much less severe than the distortion obtained with Kershaw's method.

We next solved the wave-propagation problem on a mesh that was introduced by Shestakov *et al.* [3] and is shown in Fig. 15. This mesh is not only highly skewed, but exhibits severe hourglassing as well. The parallelogram fixup associated withour scheme was invoked in seven out of the 1024 cells in the mesh. Note that evenon this highly distorted mesh, less than 1% of the cells require the parallelogram fixup. We performed calculations on this mesh in order to demonstrate the accuracy of our scheme when the parallelogram fixup is used. The steady state contour solutions for this mesh using Kershaw's method and our method

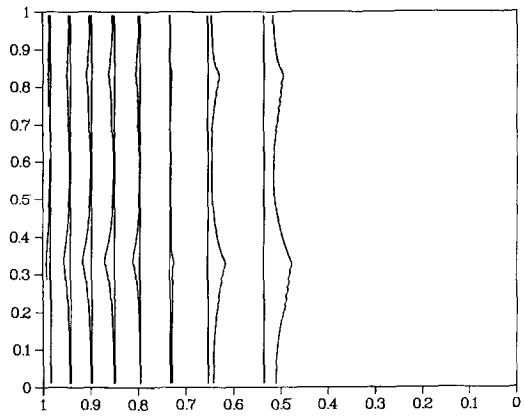

FIG. 13. Comparison of the early-time contour solution for the wave propogation problem on the "z-mesh" problem using Kershaw's method with the orthogonal mesh solution. Note that the plotting algorithm sometimes truncates contour lines near the edge of the mesh.

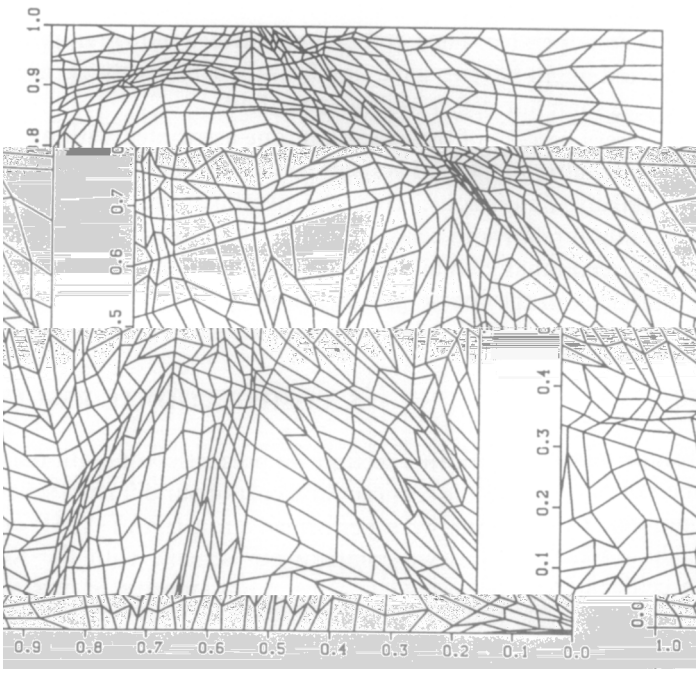

FIG. 15. The Shestakov mesh.

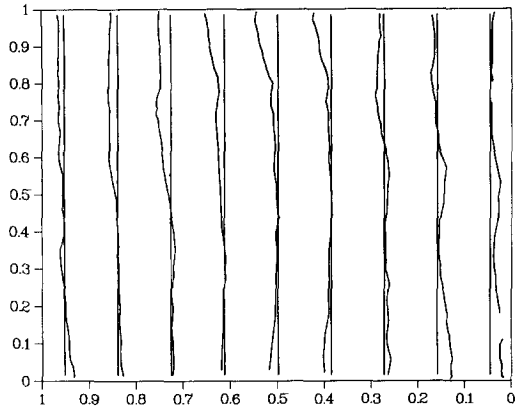

FIG. 16. Comparison of the steady-state contour solution for the wave propogation problem on the Shestakov mesh using Kershaw's method with the exact solution. Note that the plotting algorithm sometimes truncates contour lines near the edge of the mesh.

are compared with the exact solution in Figs. 16 and 17, respectively. Kershaw's scheme once again gives a solution that follows the mesh to some extent. Our scheme does not give the exact solution on this mesh, as it does on the Kershaw mesh, because the parallelogram fixup is invoked in several cells. However, the effect of the fixup is fairly localized, and the solution is considerably more accurate than that obtained with Kershaw's method.

We next performed calculations which demonstrate the accuracy of our scheme as a function of mesh refinement. We claim that our scheme gives the exact solution in the limit as the mesh is refined, regardless of the smoothness of the mesh, as long as the degree of mesh distortion is bounded in the refinement process, and the parallelogram fixup need not be invoked. Kershaw's scheme will not give a convergent solution unless the mesh becomes smooth as it is refined. This represents a significant deficiency since the meshes in realistic calculations are usually far from smooth. To demonstrate the convergence properties of our scheme and Kershaw's scheme, we performed a series of calculations on "random" meshes. An example of such a mesh is shown in Fig. 18. This mesh was generated from a uniform orthogonal mesh by randomly displacing each corner of each interior mesh cell by 20% of the original cell width. Specifically, given an initial uniform cell width of w, we place each cell corner at a random position on a circle of radius $0.2w$ centered about the original position of the corner. This procedure gives a mesh that is both skewed and hourglassed, the mesh is nowhere smooth onits interior, and the degree of mesh distortion remains relatively constant as the number of mesh cells is increased. The problem that we solved on these meshes is defined as

$$-\frac{d}{dz}\left[D\frac{d\phi}{dz}\right]=Qz^2 \tag{71}$$

for $z\in[0,1]$, with an extrapolated zero intensity at $z=1+2D$ and an extrapolated zero intensity at $z=-2D$, where and $D=\frac{1}{30}$ and $Q=1$. This one-dimensional problem is solved on a two-dimensional mesh by imposing reflective conditions along the top ($r=1$) and bottom ($r=0$) edges of the mesh. The exact solution to this problem is given by

$$\phi=a+bz+cz^4, \tag{72}$$

where

$$a=\frac{Q}{6}\left[\frac{1+8D}{1+4D}\right], \tag{73}$$

$$b=\frac{Q}{12D}\left[\frac{1+8D}{1+4D}\right], \tag{74}$$

$$c=-\frac{Q}{12D}. \tag{75}$$

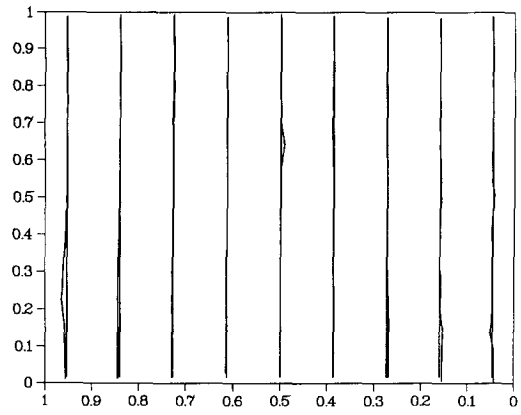

FIG. 17. Comparison of the steady-state contour solution for the wave propogation problem on the Shestakov mesh using the new method with the exact solution.

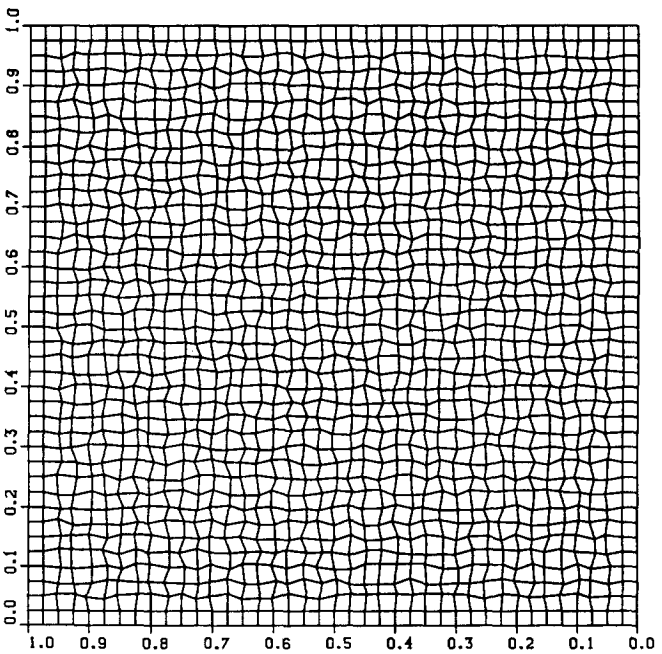

FIG. 18. The 40×40 random mesh.

We performed calculations for this problem using 10×10, 20×20, 40×40, and 80×80 random and orthogonal meshes. Calculations were performed on the orthogonal meshes with the standard five-point difference scheme (Set 1) and on the random meshes with our scheme (Set 2) and with the Kershaw scheme (Set 3). Both our method and Kershaw's method give the standard five-point difference solution on an orthogonal mesh. The errors in the numerical solutions were calculated using a standard L_2 norm:

$$\text{error} = \left[\frac{\sum_{k,l} (\phi_{k,l}^{\text{exact}} - \phi_{k,l})^2}{\sum_{k,l} (\phi_{k,l}^{\text{exact}})^2} \right]^{1/2} . \tag{76}$$

The errors for each calculation are given in Table I. Our method gives errors on the random mesh that are very comparable to those obtained on the orthogonal mesh. Most importantly, our method gives an error reduction factor of very close to four in going from the 20×20 random mesh to the 40×40 random mesh, and from the 40×40 random mesh to the 80×80 random mesh. This indicates that our method converges with second-order accuracy. As expected, Kershaw's method does not converge as the mesh is refined. Similar behavior is expected for Pert's scheme [2].

5.2. *Computational Cost*

The purpose of this section is to demonstrate the cost of our method relative to that of schemes most commonly used in production codes. A good standard of comparison for such a demonstration is the Kershaw method with a vectorized ICCG [10] solver. The efficiency of our scheme is compared in Table II to that of the Kershaw scheme with such a solver. Three calculations were performed for the wave propagation problem. The first calculation was a performed on a 48×48 Kershaw mesh with one very small time step, and the second calculation was a performed on the same mesh with one very large time step. The third calculation was performed on a 100×100 random mesh with one very large time step. It can be seen from Table II that our scheme always converges in fewer iterations than Kershaw's scheme, but our scheme is nonetheless from about five to 25 times more costly than Kershaw's scheme. The relative efficiency of our method increases as the number of mesh cells, the time step, and the orthogonality of the mesh increase. These first two factor simply increase the condition number of the diffusion matrix. In general, multigrid methods are expected to become increasingly effective relative to the ICCG methods as a system of equations becomes increasingly ill-conditioned. The third factor increases the accuracy of the approximate diffusion scheme used on the coarse grids, and thus it increases the efficiency of the multigrid scheme.

TABLE II

Comparison of Computational Efficiency

Method	CPU time	Iterations	Relative cost
	Problem 1		
New	0.51	3	25.8
Kershaw	0.02	3	1.0
	Problem 2		
New	2.89	28	20.1
Kershaw	0.14	67	1.0
	Problem 3		
New	2.96	7	4.35
Kershaw	0.68	89	1.0

The high relative cost per iteration of our scheme follows from several factors. First, our scheme has three times the global number of unknowns of Kershaw's scheme. Second, and most importantly, each line-relaxation matrix associated withour scheme has three times the bandwidth and four times the number of unknowns of that associated with Kershaw's scheme. Third, our diffusion matrix is asymmetric, necessitating the use of partial pivoting in the Gaussian elimination process and inhibiting vectorization.

In addition to the test calculations that have been discussed, a wide variety of production 1-T radiation-hydrodynamics calculations were performed on a CRAY-YMP computer using our method and Kershaw's scheme with a vectorized ICCG solver. The *total* CPU time (i.e., diffusion plus hydrodynamics) required with our method varied from about 2.5 to 5 times more than that required with Kershaw's method. This is not inconsistent with the timing results shown here because the overhead associated with the hydrodynamics calculations is usually quite large. Since 1-T calculations are generally not particularly expensive, this is not an unreasonable price to pay for increased accuracy.

Bowtie and boomerang cells have often appeared in the calculations which we have performed, and no failure of the algorithm has yet been observed. Thus it appears that our method is sufficiently robust to be used in production codes.

Comparison of Convergence Properties

Mesh	Set 1 errors	Set 2 errors	Set 3 errors
10×10	1.5×10^{-2}	1.5×10^{-2}	1.3×10^{-2}
20×20	3.7×10^{-3}	3.8×10^{-3}	5.1×10^{-3}
40×40	9.2×10^{-4}	9.6×10^{-4}	8.4×10^{-3}
80×80	2.3×10^{-4}	2.4×10^{-4}	1.1×10^{-2}

It has been suggested that the efficiency of our overall scheme might be improved by alternating between the solution techniques of multigrid and pure relaxation. However, the low overhead of our multigrid scheme relative to pure relaxation makes it difficult to develop an alternation scheme that is universally effective. For instance, several simple alternation schemes were tested in 1-T calculations, and all of these schemes were less efficient than the pure multigrid method. Since we do not have an effective alternation scheme, we currently use either the multigrid solution technique or the relaxation solution technique for the duration of a calculation.

In closing this section we consider alternatives to our method that might be more accurate than Kershaw's method, but less expensive than our method. The high cost of our scheme is primarily due to the existence of the additional cell-edge unknowns. For materially homogeneous problems, one can take differences between cell-centered intensities to obtain a nine-point scheme that has the same convergence properties as our scheme. For instance, Margolin and Tarwater have developed such a scheme [11]. Interestingly, they similarly found that mesh hourglassing generated asymmetries in the diffusion matrix. Thus the ICCG method cannot be used to solve their equations. However, a multigrid method, which would be much less costly than our method, could clearly be developed for solving their equations. Strictly speaking, their method cannot be applied to inhomogeneous problems since differences would be taken across material interfaces. However, material discontinuities could be approximately treated with empirically defined cell-edge diffusion coefficients.

As previously discussed, our parallelogram fixup scheme is closely related to a variational method [4]. Our computational experience with this variational scheme indicates that it is considerably more accurate than Kershaw's scheme. However, like the parallelogram scheme, the variational scheme will not give a convergent solution unless each cell in the mesh becomes a parallelogram as the mesh is refined. This requirement is considerably less restrictive than the requirement of mesh smoothness associated with Kershaw's scheme. Although the variational scheme has the same number of unknowns as our scheme, it produces a symmetric positive-definite diffusion matrix. Thus it seems likely that a highly efficient ICCG method could be developed to solve the variational equation.

6. CONCLUSIONS

The diffusion scheme that we have developed is significantly more accurate for problems with highly skewed meshes than existing cell-centered methods. Our scheme is also much more costly than existing methods, but this added cost is acceptable when high accuracy on highly skewed meshes is required. Thus we conclude that our method represents a valuable alternative to existing cell-centered diffusion schemes.

We stress that the utility of our scheme is predicated upon the *need* for a *cell-centered* diffusion scheme. If cell-corner unknowns are acceptable for an application, triangular finite-element methods can be expected to give the same level of accuracy as our scheme with less computational effort. Our scheme is primarily intended for use in Lagrangian hydrodynamics codes.

Although Shestakov *et al.* [3] have used triangular finite-element diffusion methods in Lagrangian hydrodymacis calculations, the interpolations and filterings required in their algorithm to achieve compatibility with the hydrodynamics scheme represent a potentially significant source of error. Thus it is possible that a cell-centered scheme and as ours, which is inherently compatible with Lagrangian hydrodynamics codes, might represent a superior alternative to their scheme. This question should be addressed in future studies.

ACKNOWLEDGMENT

This work was performed under the auspices of the U. S. Department of Energy.

REFERENCES

1. D. S. Kershaw, *J. Comput. Phys.* **39**, 375 (1981).
2. G. J. Pert, *J. Comput. Phys.* **42**, 20 (1981).
3. A. I. Shestakov, J. A. Harte, and D. S. Kershaw, *J. Comput. Phys.* **76**, 385 (1988).
4. L. A. Olvey and J. E. Morel, "A Variational Lagrangian-Mesh Diffusion Differencing Scheme," Los Alamos National Laboratory report, in preparation.
5. L. A. Hageman and D. M. Young, *Applied Iterative Methods* (Academic Press, New York, 1981).
6. J. E Dendy, Jr., *J. Comput. Phys.* **48**, 366 (1982).
7. J. E. Dendy, Jr., *Appl. Math. Comput.* **19**, 57 (1986).
8. J. E. Dendy, Jr., *Appl. Math. Comput.* **25**, 1 (1988).
9. A. Brandt and N. Dinar, in *Numerical Methods for Partial Differential Equations*, edited by S. Parter (Academic Press, New York, 1979), p. 53.
10. D. S. Kershaw, *J. Comput. Phys.* **26**, 43 (1978).
11. L. G. Margolin and A. E. Tarwater, "A Diffusion Operator for Lagrangian Meshes," Proceedings of the Fifth International Conference on Numerical Methods in Thermal Problems, Montreal, Canada, July 1987.